Supplementary information to the article:

Competing Turing and Faraday instabilities in longitudinally modulated passive resonators

François Copie,* Matteo Conforti, Alexandre Kudlinski, and Arnaud Mussot
Univ. Lille, CNRS, UMR 8523 - PhLAM - Physique des Lasers Atomes et Molécules, F-59000 Lille, France

Stefano Trillo
Department of Engineering, University of Ferrara, Via Saragat 1, 44122 Ferrara, Italy

INTRODUCTION

This supplementary information is organised as follows. In the first section, we give the details of the stability analysis for both the Turing and the Faraday instabilities. In particular we show how to arrive at Eq. (2) and (3) in the paper. Although these results are already reported in the literature for both the Turing [1] and Faraday [2] mechanism, respectively, it is useful to show how they derive from the same starting point. Moreover we propose a different (more general) approach to look at the onset of the Faraday instability. In the second section we show examples of the temporal traces corresponding to the spectra shown in the paper. In the third section we give details concerning the experimental setup. In the last section we show additional experimental results concerning bistability and hysteresis in the system.

STABILITY ANALYSIS

We consider the Lugiato-Lefever equation (LLE) in non-dimensional form [Eq. (1) of the manuscript], that we repeat here for convenience:

$$i\frac{\partial u}{\partial z} - \frac{\beta(z)}{2}\frac{\partial^2 u}{\partial t^2} + |u|^2 u = (\delta - i\alpha)u + iS, \tag{S1}$$

where the periodic dispersion profile is of the form $\beta(z) = \beta_{av} + \beta_m f(z)$, β_{av} being the average dispersion, β_m the amplitude of the modulation and $f(z)$ a periodic function of normalized period Λ (the spatial frequency is $k_g = \frac{2\pi}{\Lambda}$) with zero average and peak-to-peak amplitude equal to two [e.g. $f(z) = \sin(k_g z)$]. Since the distance z is measured in units of the cavity length, for consistency the period must be chosen as a fraction, namely $\Lambda = 1/N$ ($N = 1, 2, \ldots$).

The stationary solution of Eq. (S1), $u_0(z,t) = \sqrt{P_u}$, which can be assumed real without loss of generality, follows from the steady state response $P = P(P_u)$, explicitly $P = P_u[(P_u - \delta)^2 + \alpha^2]$, where $P = |S|^2$ is the input power and $P_u = u_0^2$ is the intracavity power. The steady state response is bistable whenever $\delta^2 > 3\alpha^2$. In this case the function $P_u(P)$ is multivalued in the range $P(P_u^+) \leq P \leq P(P_u^-)$ where $P_u^{\pm} = (2\delta \pm \sqrt{\delta^2 - 3\alpha^2})/2$ stands for the knees of the bistable response. In the multivalued region, out of the three possible solutions, only the lower and the higher ones are stable. The intermediate one, associated to a negative slope, is dynamically unstable so it is not reachable in the experiments.

The cavity steady states can destabilize through the exponential growth of modulations which can be due to a Turing (modulation instability, MI) or Faraday (parametric instability) mechanism, respectively. The Turing instability is characteristic of a uniform cavity (in a periodic case it is affected only by the average quantities), whereas the Faraday instability is a consequence of the parametric resonance due to the forcing, and hence the characteristics of the instability are affected by the period and the strength of the perturbation. However both follows from a linear stability analysis of the steady solution u_0, which at some point needs to be specialized to describe the two mechanisms. To this end, we start by considering the evolution of a perturbed solution $u(z,t) = \sqrt{P_u} + [u(z,t) + iv(z,t)]$, where we assume the real functions $u, v \ll u_0$.

By linearization of Eq. (S1), we obtain a linear system of PDE ruling the evolution of the perturbation:

$$\frac{\partial u}{\partial z} - \frac{\beta(z)}{2}\frac{\partial^2 v}{\partial t^2} + (P_u - \delta)v + \alpha u = 0, \tag{S2}$$

$$\frac{\partial v}{\partial z} + \frac{\beta(z)}{2}\frac{\partial^2 u}{\partial t^2} - (3P_u - \delta)u + \alpha v = 0. \tag{S3}$$

Taking the Fourier transform in time [$\hat{u}(z,\omega) = \int u(z,t)e^{i\omega t}dt$] of this system leads, for each frequency, to a second order ODE system

$$\frac{d}{dz}\begin{bmatrix}\hat{u}\\ \hat{v}\end{bmatrix} = \begin{bmatrix}-\alpha & -g(z)\\ h(z) & -\alpha\end{bmatrix}\begin{bmatrix}\hat{u}\\ \hat{v}\end{bmatrix}, \tag{S4}$$

where $g(z) = \frac{\beta(z)}{2}\omega^2 + P_u - \delta$ and $h(z) = \frac{\beta(z)}{2}\omega^2 + 3P_u - \delta$.

Uniform cavity: Turing instability

We start to consider a uniform cavity, where $\beta_m = 0$, $\beta(z) = \beta_{av}$. System (S4) is similar to a damped harmonic oscillator, whose oscillation spatial frequency (wavenumber) is

$$k_{av} = \sqrt{h_{av}g_{av}} = \sqrt{\left(\frac{\beta_{av}}{2}\omega^2 + 2P_u - \delta\right)^2 - (P_u)^2}. \tag{S5}$$

Its eigenvalues, which rule the z evolution, read $-\alpha \pm ik_{av}$. When the detuning δ is sufficiently high, k_{av} can become imaginary in a certain range of ω, and the solution of Eqs. (S4) involves two exponentials with real argument. In this range, if $|k_{av}| > \alpha$ the perturbations $\hat{u}, \hat{v}$ grows exponentially $\propto \exp[g(\omega)z]$ with growth rate $g(\omega) = -\alpha + \sqrt{-h_{av}g_{av}}$, entailing MI (Turing) of the stationary solution [1]. The most unstable Turing frequency $\omega = \omega_T$ and its corresponding gain, can be easily calculated from the eigenvalues to be

$$\boxed{\omega_T = \sqrt{\tfrac{2}{\beta_{av}}(\delta - 2P_u)},\ \ g(\omega_T) = P_u - \alpha.} \tag{S6}$$

We recall that, unlike the cavityless fiber configuration, where MI occurs only in the anomalous GVD regime and without threshold, in the cavity MI occurs also with normal GVD and has a threshold $P_u = \alpha$, obtained by imposing $g = 0$ in Eq. (S6).

The linear stability analysis presented here allows to determine the conditions of instability with respect to small perturbations but does not provide any information on the dynamics of large amplitude modulated states. In other words, MI is the generating mechanism of the Turing pattern but only in a subset of the unstable region, the growth of the sideband can generate a stable pattern. This has been analyzed in details in [4]. The region of parameter where MI can lead to the generation of a stable Turing pattern is highlighted in green in Fig. 1(d) of the manuscript.

Periodically modulated cavity: Faraday instability

Before proceeding with the analysis, it is useful to factorize the effect of the losses through the transformation $[\hat{u}, \hat{v}] = [\tilde{u}, \tilde{v}]\exp(-\alpha z)$, that transforms Eqs. (S4) into a one degrees of freedom Hamiltonian system with canonical coordinates $[\tilde{u}, \tilde{v}]$:

$$\frac{d}{dz}\begin{bmatrix}\tilde{u}\\ \tilde{v}\end{bmatrix} = \begin{bmatrix}0 & -g(z)\\ h(z) & 0\end{bmatrix}\begin{bmatrix}\tilde{u}\\ \tilde{v}\end{bmatrix}. \tag{S7}$$

Since the coefficients in the equation are z-periodic with period Λ, Floquet theory applies. This amounts to study the evolution over one period Λ, to obtain the Floquet map Φ which is the two by two real matrix defined by $[\tilde{u}(\Lambda), \tilde{v}(\Lambda)]^T = \Phi[\tilde{u}(0), \tilde{v}(0)]^T$. As a result $[\tilde{u}(n\Lambda), \tilde{v}(n\Lambda)]^T = \Phi^n[\tilde{u}(0), \tilde{v}(0)]^T$. Note that Φ necessarily has determinant one, since it is obtained by integrating a Hamiltonian dynamics, which preserves phase space volume. As a consequence, the two eigenvalues of Φ are constrained to lie either both on the unit circle, or both on the real axis. Only in the latter case the system can be unstable, the instability being associated with $|\lambda| > 1$ according to Floquet theory.

Since the system (S7) is not autonomous, it cannot be solved analytically in general. Nevertheless, the above observations will allow us to obtain some information about its (in)stability for (relatively) small β_m, which, importantly, hold valid regardless of the specific shape of the forcing $f(z)$ [3].

To see this, let us start from the unperturbed limit $\beta_m = 0$, $\beta(z) = \beta_{av}$. It is then straightforward to integrate the system (S7). The Floquet map is then given by

$$\Phi_{av} = \begin{bmatrix}\cos(k_{av}\Lambda) & -\dfrac{g_{av}}{k_{av}}\sin(k_{av}\Lambda)\\ \dfrac{k_{av}}{g_{av}}\sin(k_{av}\Lambda) & \cos(k_{av}\Lambda)\end{bmatrix}. \tag{S8}$$

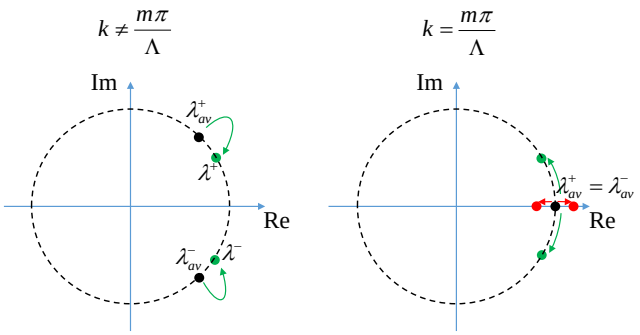

FIG. S1. Sketch illustrating, in the complex plane, the effect of the forcing term $f(z)$ on the eigenvalues of the Floquet map (S8). Black dots correspond to the unperturbed eigenvalues lying on the unit circle (dashed line). Colored dots show the new position of the eigenvalues after switching on the perturbations, leading to a stable regime when $k \neq \frac{m\pi}{\Lambda}$ (left sketch) and an unstable one when $k = \frac{m\pi}{\lambda}$ (right sketch).

The eigenvalues of Φ_{av} can be easily computed as

$$\lambda^{\pm}_{av} = \exp(\pm i k_{av} \Lambda). \tag{S9}$$

We assume that $k_{av}(\omega)$ is real, i.e. the uniform cavity is stable with respect to perturbations at frequency ω, and ask ourselves what happens by switching on the periodic dispersion described by $f(z)$. The system (S7) becomes non-autonomous and hence it is no longer possible, in general, to give a simple closed form expression of the eigenvalues. Nevertheless, we do know that, for sufficiently small β_m, the eigenvalues of Φ must be close to the eigenvalues $\lambda^{\pm}_{av}$. We then distinguish two cases:

1. Off-resonant case $k_{av} \neq \frac{m\pi}{\Lambda}$. Since $k_{av}\Lambda \neq m\pi$, it follows from Eq. (S9) that $\lambda^-_{av} = (\lambda^+_{av})^*$, *are distinct and they both lie on the unit circle, away from the real axis.* They then must remain on the unit circle under perturbation since, for the reasons explained above, they cannot move into the complex plane away from the unit circle. A pictorial description of this situation is shown in the left panel of Fig. S1. In this case, the stationary solution is linearly stable under a sufficiently small perturbation $\beta_m f(z)$ and this statement does not depend on the precise form of $f(z)$.

2. On-resonant case $k_{av} = \frac{m\pi}{\Lambda}$**.** It follows from Eq. (S9) that $\lambda^+_{av} = \lambda^-_{av} = \pm 1$ (upper or lower sign holds for m even or odd, respectively) is a doubly degenerate eigenvalue of Φ_{av}. Under a small perturbation, the degeneracy can be lifted and two real eigenvalues can be created, one greater than one, one less than one in absolute value. The system has then become unstable! A pictorial description of this situation is shown in the right panel of Fig. S1. In principle, under very peculiar perturbations, the eigenvalues might also move along the circle implying that the system remain stable. However, for the most common perturbations (sinusoidal, square wave, sawtooth, comb, ...), the system destabilizes under an arbitrarily small perturbation, following the split of the eigenvalues on the real axis at the degenerate points ± 1.

We recap by saying that, when the forcing is switched on, the instability sets in under the resonant condition $k_{av} = \frac{m\pi}{\Lambda}$. Recalling the expression of $k_{av} = k_{av}(\omega)$ in Eq. (S5), it is straightforward to show that the $m-$th order resonance is fulfilled at frequency $\omega = \omega_m$, where

$$\boxed{\omega_m = \sqrt{\left\{\frac{2}{\beta_{av}}(\delta - 2P_u)\right\} \pm \left[\frac{2}{\beta_{av}}\sqrt{\left(\frac{m\pi}{\Lambda}\right)^2 + P_u^2}\right]},} \tag{S10}$$

which is therefore the frequency at which the system destabilizes for an infinitely small Hamiltonian perturbation of Φ_{av}.

In Eq. (S10) it is possible to recognize the contribution of the periodic dispersion in the term in the square bracket.

We emphasize that the resonance condition

$$\boxed{k_{av}(\omega_m) = m\frac{\pi}{\Lambda} = m\frac{k_g}{2}} \tag{S11}$$

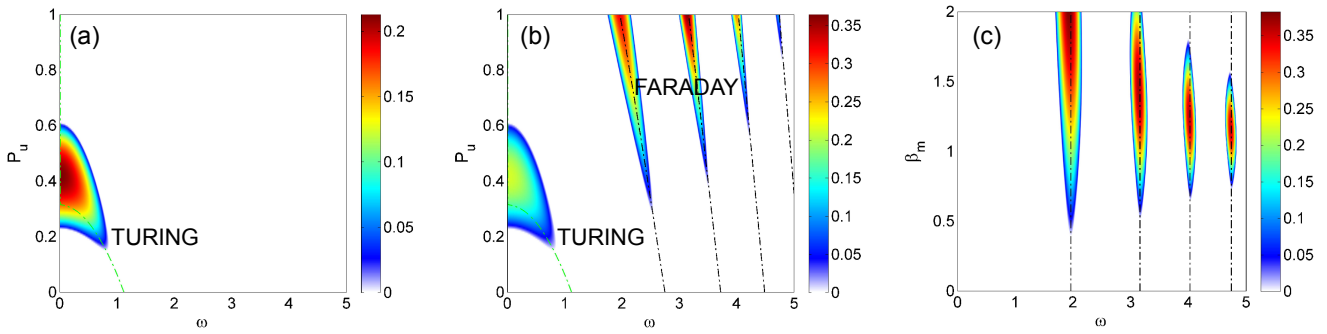

FIG. S2. Color level plot of growth rate $g(\omega)$. (a) Uniform cavity $\beta_{av} = 1$, $\beta_m = 0$, $\Lambda = 1$. The dashed green curve indicates the peak gain calculated from Eq. (S6). (b) Modulated cavity $\beta_{av} = 1$, $\beta_{a,b} = 1 \pm 1.5$, $\Lambda_a = \Lambda_b = 0.5$. The dashed black curves indicates the peak gain calculated from Eq. (S10) for $m = 1, 2, 3, 4$. (c) Modulated cavity $\beta_{av} = 1$, $P_u = 1$, $\Lambda_a = \Lambda_b = 0.5$. In all three plots, $\delta = \pi/5$, $\alpha = 0.15$.

is the condition of *parametric resonance, i.e. the natural spatial frequency of the unperturbed harmonic oscillator (k_{av}) is equal to a multiple of half the forcing spatial frequency (π/Λ).*

Note that in the case of extended systems exhibiting spatial pattern formation, the role of ω and k is interchanged, and one can say that, under forcing of the system at frequency ω_d, the system develops a parametric instability characterized by wavenumbers k_m, selected through the dispersion relation $\omega = \omega(k)$ (seen by the linearized perturbation of the steady-state) in such a way that the resonance conditions $\omega(k_m) = m\omega_d/2$ are fulfilled.

We return now to the original (damped) system for the perturbations $[\hat{u}, \hat{v}]$. The Floquet map is simply given by $\Psi_{av} = \exp(-\alpha\Lambda)\Phi_{av}$, whose eigenvalues read as:

$$\sigma_{av}^{\pm} = \exp(-\alpha\Lambda)\lambda_{av}^{\pm} = \exp[(-\alpha \pm ik_{av})\Lambda]. \tag{S12}$$

That means that the eigenvalues $\sigma_{av}^{\pm}$ lie in the complex plane either on a circle of radius $\exp(-\alpha\Lambda)$ (case 1), or on the real axis (case 2). Now the perturbation can grow only if the forcing β_m is sufficient to push one of the eigenvalues outside the unit circle. In this case, the perturbations $\hat{u}, \hat{v}$ will experience an exponential growth with rate $g(\omega) = \ln(\max|\sigma^{\pm}|)/\Lambda$. This means that there is a threshold on β_m for the onset of the parametric instability. On the same footing, for a fixed β_m, there exist a power threshold for the parametric instability to appear.

To summarize, the Faraday instability appears in general at multiple frequencies ω_m given by Eq. (S10) which depend on the period of the forcing and represent the tips of the unstable regions known as Arnold tongues, whereas a threshold in the strength of the forcing (or intracavity power) exists which depends on the losses (the higher the losses, the higher the threshold) and on the specific shape of the perturbation (though no general analytical formulas can be given for the threshold).

The stability analysis presented here allows to determine the conditions of parametric instability with respect to small perturbations but does not provide any information on the dynamics of large amplitude modulated states. In other words, parametric instability is the generating mechanism of the Faraday pattern but only in a subset of the unstable region the growth of the sideband can generate a stable pattern. The region where parametric instability can lead to the generation of a stable Faraday pattern is highlighted in blue in Fig. 1(d) of the manuscript, and it was calculated from numerical simulation of LLE. Above this region, the Faraday pattern becomes unstable and the behavior of the cavity chaotic.

Piecewise constant dispersion

An example of practical interest where the Floquet analysis can be performed *analytically* is a cavity with a piecewise constant dispersion [2]. This case corresponds to the experimental set-up we used, where the intracavity loop is made of two pieces of different fibers spliced together. The Floquet map is given by

$$\Psi = \exp(-\alpha\Lambda)\Phi_a\Phi_b, \tag{S13}$$

where $\Phi_{a,b}$ has the expression (S8) calculated for a dispersion $\beta(z) = \beta_{a,b}$, where the two pieces of fiber has length $\Lambda_{a,b}$, such that $\Lambda_a + \Lambda_b = \Lambda$ and the average dispersion is $\beta_{av} = (\beta_a\Lambda_a + \beta_b\Lambda_b)/\Lambda$.

The eigenvalues of Ψ are given by

$$\sigma^{\pm} = \frac{\Delta}{2} \pm \sqrt{\frac{\Delta^2}{4} - W}, \tag{S14}$$

where

$$\Delta = e^{-\alpha\Lambda}\left[2\cos(k_a\Lambda_a)\cos(k_b\Lambda_b) - \frac{g_a h_b + g_b h_a}{k_a k_b}\sin(k_a\Lambda_a)\sin(k_b\Lambda_b)\right], \tag{S15}$$

and $W = e^{-2\alpha\Lambda}$. We have parametric instability if $|\Delta| > (1+W)$, with gain $g(\omega) = \ln(\max|\sigma^{\pm}|)/\Lambda$.

In Fig. S2 we report some examples of analytically calculated instability gain. Figure S2(a) shows the gain as a function of perturbation frequency and intracavity power for a homogeneous cavity. In this case, we observe a branch located around zero frequency, that can generate a stable Turing pattern. Figure S2(b) shows the gain for a modulated cavity in the same operating conditions. The Turing branch survives, and we see the generation of several branches due to the periodic forcing. This parametric instability branches (also called Arnold tongues) are the generating mechanism for the Faraday patterns. The existence of both Turing and Faraday branches in the same device allows us to observe the competition between the two phenomena. Figure S2(c) shows the Arnold tongues as a function of the forcing amplitude β_m for a fixed power. Due to nonzero losses α, there exist a threshold for the onset of the instability (as discussed above), which is generally different for each tongue.

SIMULATED TEMPORAL TRACES

Four typical temporal profiles corresponding to our experiments are displayed in Fig. S3. These figures have been obtained from numerical simulations of the LLE since their characteristic time scale lies in the ps regime, and it is thus impossible to measure it experimentally even with ultra-fast oscilloscopes.

In all cases, a stable pattern is obtained after a few hundred roundtrips consisting in a periodic modulation of the power on top of a constant background. We emphasize that the large difference of period between panels (c) and (d) reflects the diversity in frequencies of the sidebands of Turing and Faraday patterns, respectively, which is the distinctive trait which allows us to unequivocally identify the transition in Fig. 5(b) of the paper.

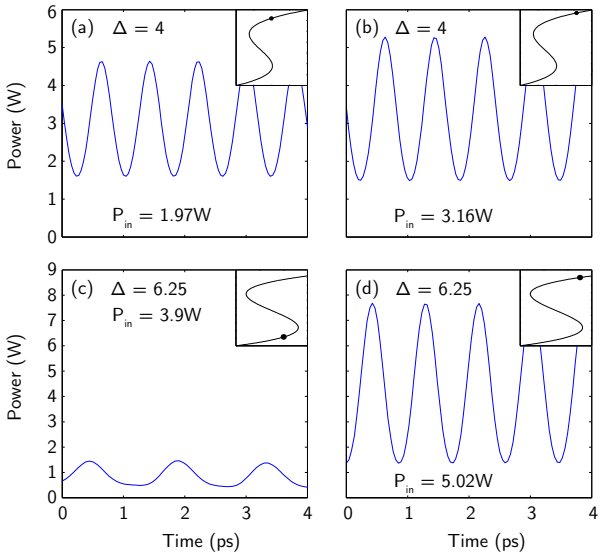

FIG. S3. Temporal traces corresponding to the input powers and detunings of our experiments (Figs. 3 and 4 in the paper). The insets show the corresponding workpoint over the bistable response.

EXPERIMENTAL SETUP

In our experiments the fiber resonator is pumped by a cw-laser which is intensity-modulated using an electro-optic modulator (EOM) to generate 4 ns long pulses, which are few thousands time longer that the typical period of the modulated structure to observe. This allows suppression of Brillouin scattering effects and reaching large peak powers after passage through two erbium-doped fiber amplifiers (EDFAs) combined with fiber Bragg gratings (FBGs) to minimize the impact of amplified spontaneous emission from the EDFAs. The repetition rate is set to 4.14 MHz corresponding to the roundtrip time of the 51.6 m long cavity (only one pulse circulates inside the cavity per roundtrip). This "Nonlinear beam" is launched inside the cavity through the 90/10 SMF coupler (i.e., at each roundtrip, 10% of external and intracavity powers are coupled in and out, respectively). The spectrum at the output of the cavity is recorded by an optical spectrum analyser (OSA). We estimate the total cavity losses from the relation $\alpha = \pi/\mathcal{F}$, where $\mathcal{F}$ is the finesse of the cavity, which we measure from cavity transmission [Fig. 2(c) of the manuscript] to be $\mathcal{F} \approx 20$, yielding typically $\alpha \approx 0.157$.

In order to operate at constant detuning δ we extract a small fraction of the pump power in the "Control beam", which is launched inside the cavity in the counterpropagating configuration with respect to the "Nonlinear beam". We control the linear phase accumulation of light during a roundtrip by finely tuning the wavelength of the laser. The output of the "Control beam" is launched into a servo controlled system (PID) to be compared to a reference level related to the desired detuning. It then generates an error signal that finely tunes the pump wavelength to compensate for the environmental fluctuations, and thus locks the value of the detuning. The maximum duration of the locking is strongly linked to the environment fluctuations for they eventually lead to a failure of the PID system. The interested reader may find additional informations concerning the operation of the cavity and the cavity-detuning control scheme in [5]. In this reference, the authors were able to stabilize the detuning by finely stretching the fiber inside the cavity, which is somehow equivalent to the method used here.

We also point out that since the dispersion map is made by splicing together two different fibers, we have also an effective map in the nonlinearity due to the different nonlinear coefficients, namely 1.2 $(\text{W km})^{-1}$ for the SMF28 and 5.6 $(\text{W km})^{-1}$ for the DSF. This can be easily accounted for in the theory. However, our numerical check reveals that the contribution of the periodicity of the nonlinearity is negligible compared to the dispersion contribution. Therefore, for the sake of simplicity, the theory in the paper was presented by referring to the dispersion map, which is the dominant contribution to the Faraday instability.

EXPERIMENTAL OBSERVATION OF HYSTERESIS

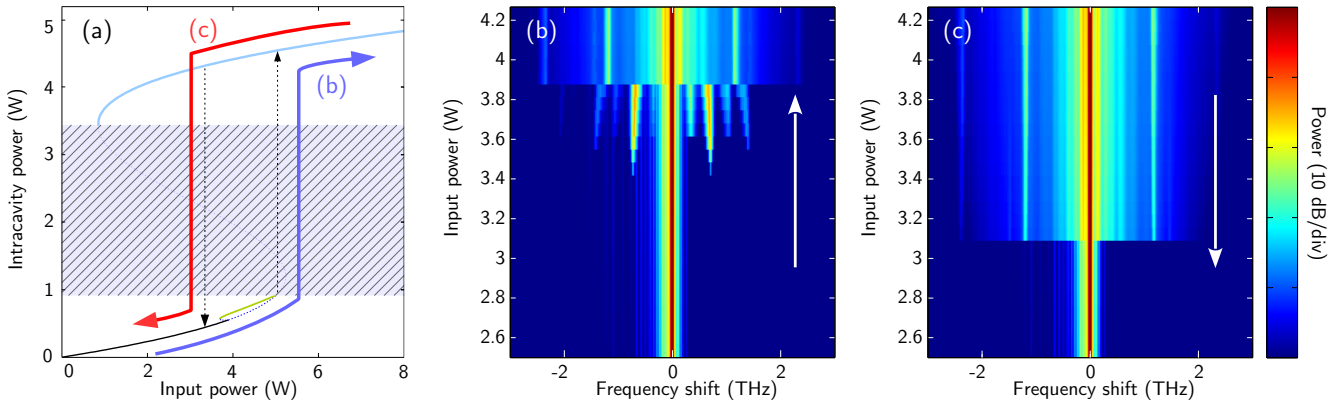

FIG. S4. (a) Bistable response of the cavity calculated for $\Delta = 6.25$, along with a sketch of the hysteresis loop.(b) Experimental spectra at the output of the cavity when progressively increasing the input power [blue path in panel (a)]. (c) Experimental spectra at the output of the cavity when progressively decreasing the input power starting from the upper branch [red path in panel (a)]. The white arrows give the direction of changes in power.

In the manuscript we focus our attention on the evolution of the spectrum when increasing the power at the input of the cavity. In this section we report additional experimental results showing that the system experiences

unconventional hysteresis (provided that the pumping of the cavity fulfills sufficient synchronicity conditions [4]). The hysteresis is the only measurable consequence of the existence of the negative slope branch of the stationary response of the cavity, and manifests itself in a diversity of the power threshold corresponding to up-switching and down-switching, respectively. This behavior is qualitatively illustrated in the theoretical sketch in Fig. S4(a). In our case the hysteresis loop involves (in sequence) the lower stable branch, the onset of Turing instability on this branch, the jump to the parametrically (Faraday) unstable upper branch, and the return to the lower stable branch. Indeed, in the experiment, when we increase the power, we first observe the sidebands characteristic of the Turing instability up to the point where the system jumps on the upper branch, thus exhibiting sidebands with higher frequency (Faraday instability) [see Fig. S4(b), identical to Fig. 5(b) of the manuscript]. From this point, if we decrease the power, we observe the spectral evolution illustrated in Fig. S4(c). The system follows the upper branch and Faraday instabilities are sustained to input powers below the primary (Turing) threshold on the lower branch. The system then falls back to the modulationally stable part of the lower branch. Note the slight narrowing of the sidebands when decreasing the input power in agreement with the prediction of the Floquet theory [see Fig. 4(b) of the manuscript]. The result in Fig. S4 further proves the bistable nature of our system.

* francois.copie@univ-lille1.fr

[1] M. Haelterman, S. Trillo, and S. Wabnitz, Opt. Lett. **17**, 745 (1992); Opt. Commun. **91**, 401 (1992).
[2] M. Conforti, A. Mussot, A. Kudlinski, and S. Trillo, Opt. Lett. **39**, 4200 (2014).
[3] S. Rota Nodari, M. Conforti, G. Dujardin, A. Kudlinski, A. Mussot, S. Trillo, and S. De Biévre, Phys. Rev. A **92**, 013810 (2015).
[4] S. Coen, M. Haelterman, P. Emplit, L. Delage, L. M. Simohamed, and F. Reynaud, J. Opt. B: Quantum Semiclass. Opt **1**, 36 (1999).
[5] S. Coen, M. Haelterman, P. Emplit, L. Delage, L. M. Simohamed, and F. Reynaud, JOSA B **15**, 2283 (1998).